Appl. Phys. A (2017) 123:529
DOI 10.1007/s00339-017-1145-5

Applied Physics A
Materials Science & Processing

Facile electrosynthesis and characterization of superparamagnetic nanoparticles coated with cysteine, glycine and glutamine

Mustafa Aghazadeh[1] · Isa Karimzadeh[2] · Taher Doroudi[3] · Mohammad Reza Ganjali[4] · Peir Hossein Kolivand[3] · Davoud Gharailou[4]

Received: 21 January 2017 / Accepted: 13 July 2017 / Published online: 19 July 2017

Abstract A novel and facile strategy has been developed for the preparation of cysteine-, glycine- and glutamine-coated magnetite nanoparticles (MNPs). According to this strategy, Fe_3O_4 nanoparticles were electrodeposited from an aqueous electrolyte containing a dissolved iron salt and amino acids. A simple deposition mode i.e., constant current and two-electrode set-up was used in the electrosynthesis procedure. The magnetite phase of the deposited nanoparticles was confirmed through XRD and FT-IR analyses. Morphological observations through FE-SEM and TEM confirmed the formation of spherical MNP particles with an average size of 10 nm. The formation of cysteine, glycine and glutamine layers on the surface of the electro-synthesized particles was proved based on FT-IR, DLS and TG data. Vibrating sample magnetometery (VSM) measurements confirmed the prepared iron oxide nanoparticles to have a super-paramagnetic nature, since they exhibit a high saturation magnetization ($Ms \approx 58$ emu g^{-1}), as well as, negligible remnant magnetization (Mr) and coercivity (Ce). Based on the obtained results, the proposed platform can be considered as a fast, simple and efficient method for the preparation of surface-coated magnetite nanoparticles.

1 Introduction

Iron oxides nanoparticles with biocompatible surface chemistry and sizes less that 100 nm are promising candidates for therapeutic and diagnostic applications in biomedical sciences such as cell targeting and separation, magnetic resonance imaging (MRI), cancer therapy, hyperthermia, gene and drug delivery [1]. Among different forms of iron oxides, magnetite nanoparticles (MNPs) possess unique characters which depend on their size, surface chemistry and magnetic properties. Biomedical applications require surface engineered MNPs with special coatings, which should be nontoxic and biocompatible with the ability of targeted delivery of materials to a specified point in the body. Up to now, a variety of surface coating agents such as polymers [2–6], polysaccharides [7, 8], silica [9] and amino acids [10–14] have been used on the surface of MNPs during their preparation procedure. The type of the surface coatings and their configuration on the surface of the MNPs dedicate their overall size, surface charge, cytoxicity, magnetic performance, bio-distribution, bio-compatibility and bio-performance [14, 15]. Amino acids can be interesting agents for coating the surfaces of MNPs, due to their appropriate bio-compatibility, stabilization and important role in the body [12, 13, 16–18]. It has been reported that amino acids can stabilize iron oxide NPs better and have no considerable effects on their size and magnetic behaviors [19, 20]. Amine functionalization can improve the interactions of MNPs with large, negatively charged cell membrane domains and hence increase the chance of surface interactions. It has also been reported

✉ Mustafa Aghazadeh
maghazadeh@aeoi.org.ir

[1] Materials and Nuclear Research School, Nuclear Science and Technology Research Institute (NSTRI), P.O. Box 14395-834, Tehran, Iran

[2] Department of Physics, Faculty of Science, Central Tehran Branch, Islamic Azad University, Tehran, Iran

[3] Shefa Neuroscience Research Center, Khatam Ol Anbia Hospital, Tehran, Iran

[4] Faculty of Chemistry, Center of Excellence in Electrochemistry, University of Tehran, Tehran, Iran

that amino acids could easily attach to the surface of iron oxides through their carbonyl groups [21, 22], where the functional groups participating in the side-chains can provide active sites for further functionalization with various biological molecules and drugs for recognition and therapy applications. Hence, amino acid coating of iron oxide nanoparticles can be an increasingly interesting subject in the area of nanobiomedicine.

So far, both naked and surface-coated iron oxide nanoparticles have been prepared through different chemical routes including biosynthesis [23, 24], co-precipitation [25–27], thermal decomposition [28], hydrothermal [29–33] and sol–gel [9], laser ablation [34] methods. Beside these methods, electrochemical methods can be applied for the preparation of iron oxide nanoparticles because of their proved advantages of facility and ability to control the purity, crystallinity and size of the obtained samples, which can be actualized by manipulating the applied electrochemical parameters such as current, potential, electrolyte composition, pH and concentration [35–45]. However, electrochemical approaches, e.g., cathodic electrosynthesis have been rarely used for the preparation of surface-coated iron oxide nanoparticles.

Here, we wish to report a cathodic deposition procedure as a novel and efficient approach for the preparation of cysteine-, glycine- and glutamine-coated iron oxide nanoparticles. The synthesized magnetite NPs were characterized by XRD, FT-IR, DLS, FE-SEM, TEM, TGA and VSM techniques and the obtained data confirmed that the coated MNPs have appropriate characters for use in the area of biomedicine.

2 Experimental procedure

2.1 Materials

Ferrous chloride tetra hydrate ($FeCl_2{\cdot}4H_2O$, 99%), ferric nitrate tetra hydrate [$Fe(NO_3)_3$, 99.9%], cysteine (≥99%), glycine (≥99%) and glutamine (≥99%) were from Sigma Aldrich. All materials were used as received and without any purification.

2.2 Electrosynthesis of naked Fe_3O_4 nanoparticles

The naked magnetite nanoparticles were prepared through the cathodic electrochemical deposition (CED) method. The deposition experiments were performed using an electrochemical workstation system (Potentiostat/Galvanostat, Model: NCF-PGS 2012, Iran). The electrochemical cell used a stainless-steel cathode centered between two graphite anodes. An aqueous solution of mixed iron(III) nitrate and iron(II) chloride (0.005 M with 2:1 molar ratio) was prepared and used as the electrolyte without any additives. The naked Fe_3O_4 samples were deposited by applying a current density of 10 mA cm^{-2} for 1 h. At the end of the deposition experiments, the steel cathode was removed from the electrolyte and washed several times with distilled water. Then, the black deposit on the surface of steel electrode was scraped and subjected to the purification process, which included being repeatedly washed times with water, dispersion in ethanol and centrifugation at 6000 rpm for 20 min, followed by separation from the ethanol solution using a magnet, and drying at 70 °C in a vacuum oven for 1 h. The obtained black powder was referred to as naked nanoparticles.

2.3 Electrosynthesis of coated Fe_3O_4 nanoparticles

An electrochemical procedure similar to that used for the preparation of naked Fe_3O_4 nanoparticles was used. The only difference was that the composition of the electrolyte was changed through adding the coating agents. To this end about 1 g of each amino acid (cysteine, glycine or glutamine) was added to 1 l of water and dissolved under magnetic stirring for 10 min to prepare three different amino acid solutions. Then 2.4 g of $Fe(NO_3)_3$ and 1.6 g of $FeCl_2$ were added into each amino acid solution and stirred by a magnet for 30 min. The obtained mixtures were used as the deposition electrolytes. The electrosynthesis experiments were performed in the electrolytes by applying 10 mA cm^{-2} for 30 min. After the deposition, the steel cathode was rinsed with distilled water several times and the black deposit formed on its surface was scraped. Then (1) the deposit was washed several times with ethanol to remove the free amino acid molecules (2) it was dispersed in ethanol and centrifuged at 6000 rpm for 10 min, and (3) finally, the black powder was separated from ethanol using a magnet, and dried in a vacuum oven. The obtained black powder was labeled as amino acid-coated NPs (i.e., cysteine-, glycine- and glutamine-coated NPs) and evaluated by various characterization techniques.

2.4 Characterization of the nanoparticles

2.4.1 Size, phase and morphological analysis

The size and morphology of the prepared MNPs were studied using a field emission scanning electron microscope (FE-SEM, Mira 3-XMU with applicable voltage of 100 kV). Transmission electron microscopy (TEM, Zeiss EM 900 with accelerating voltage of 80 kV) was also used to better determine the size of the MNPs. The crystal phase and structure of the prepared MNPs were determined by powder X-ray diffraction [XRD, a Phillips PW-1800 diffractometer with Co Kα radiation ($\lambda = 1.789$ Å)]. Using

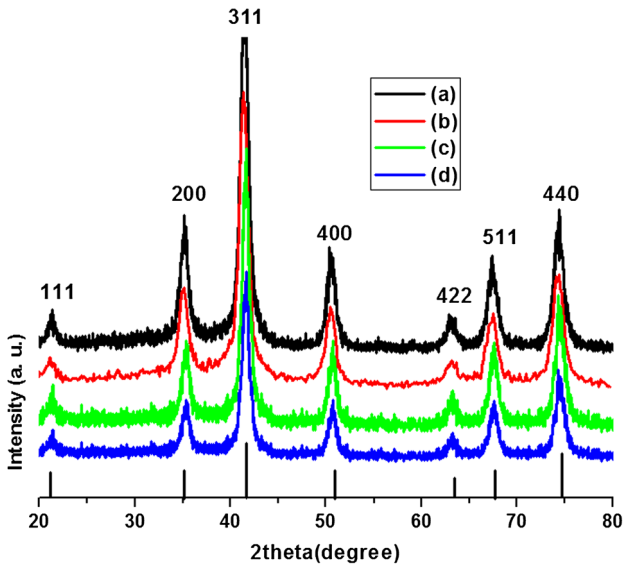

Fig. 1 XRD patterns of the prepared **a** naked, **b** cysteine-, **c** glycine- and **d** glutamine-coated Fe_3O_4 nanoparticles. *Solid lines* show diffractions of magnetite phase with reference card no. 88-0315

the diffraction patterns, the size of the crystallites was also calculated from the width of the peak profile using the Scherrer equation. The hydrodynamic diameter and zeta potentials of the prepared nanoparticles were determined by dynamic light scattering (DLS, 4700 Malvern Instruments, UK), and the measurements were conducted on the as-prepared dispersions of the naked and coated NPs [with concentration of 0.1 mg (Fe) per liter] without any filtration or centrifugation steps.

2.4.2 *Surface characterization*

The amino acid coating on the surface of the NPs, obtained through the CED process, was studied through different surface characterization techniques including FT-IR and TGA analyses. The FTIR spectra were obtained using a Bruker Vector 22 Fourier transformed infrared spectroscope. Each FTIR spectrum was collected after 20 scans at a resolution of 4 cm^{-1} from 400 to 4000 cm^{-1}. The thermal behavior analyses were also conducted under an N_2 atmosphere between the room temperature and 600 °C at a

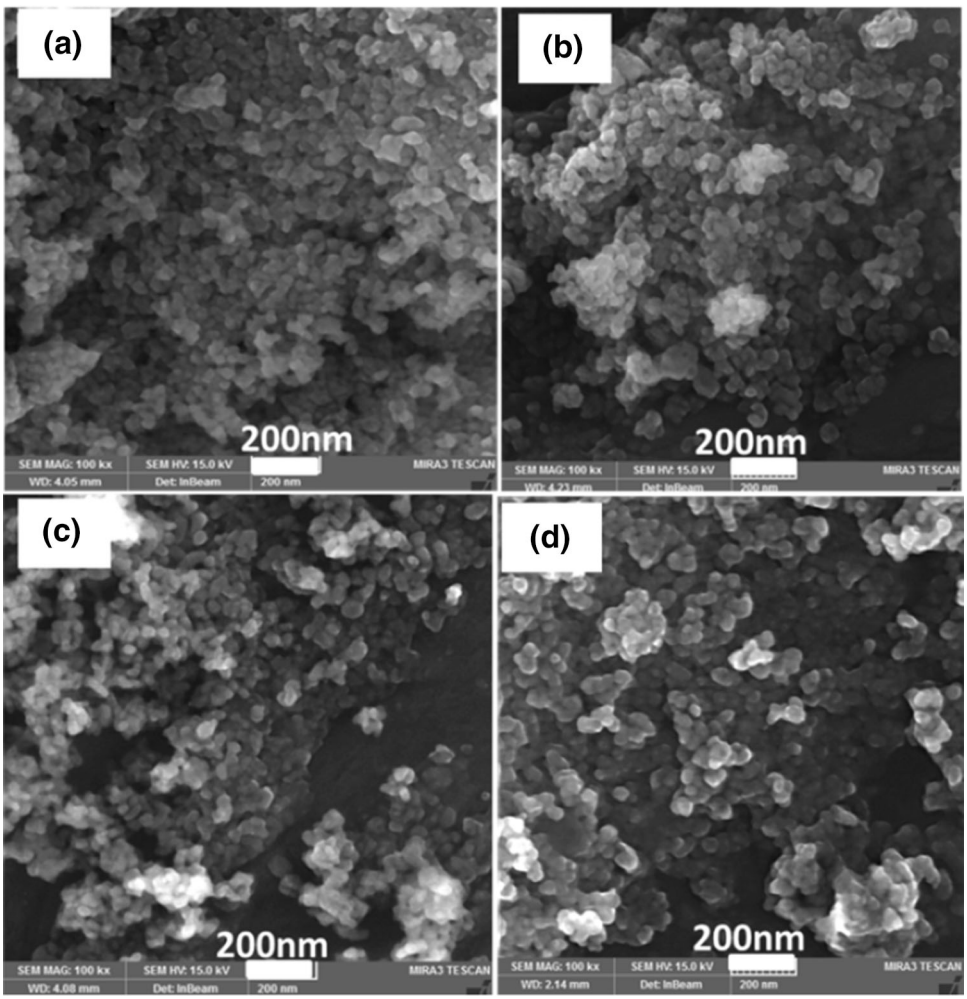

Fig. 2 FE-SEM images of the prepared nanoparticles; **a** naked, **b** cysteine-, **c** glutamine and **d** glycine-coated Fe_3O_4 nanoparticles

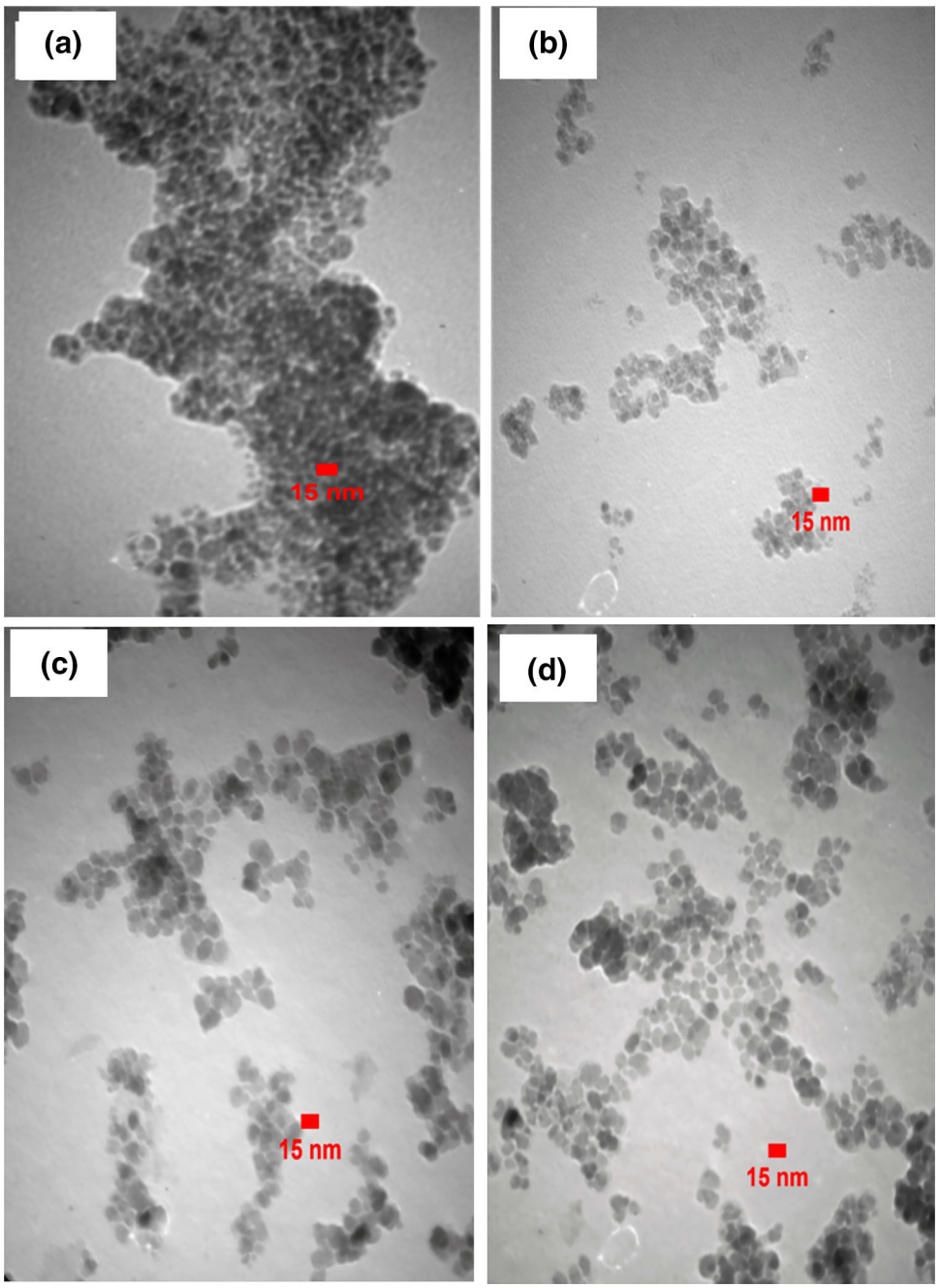

Fig. 3 TEM images of the prepared nanoparticles; **a** naked, **b** cysteine-, **c** glutamine and **d** glycine- coated Fe_3O_4 nanoparticles

heating rate of 5 °C min^{-1} using an STA-1500 Thermo-analyzer system.

2.4.3 Characterization of the magnetic properties

The magnetic properties of the prepared naked and coated NPs were assessed in the range of −20,000 to 20,000 Oe at room temperature using vibrational sample magnetometer (VSM, model: Meghnatis Daghigh Kavir, Iran). Both the magnetic hysteresis and saturation magnetization of the naked and coated MNPs were studied.

3 Results and discussion

3.1 X-ray diffraction

Figure 1 depicts the XRD patterns of the electrodeposited naked and coated iron oxide nanoparticles. The positions and relative intensities of all diffraction peaks in these XRD patterns very well match with a cubic spinel structure of magnetite (i.e., Fe_3O_4, JCPDS 01-088-0315). No extra peak is observed, which implies that all the deposited nanoparticles were composed of pure Fe_3O_4 phase. It was found that

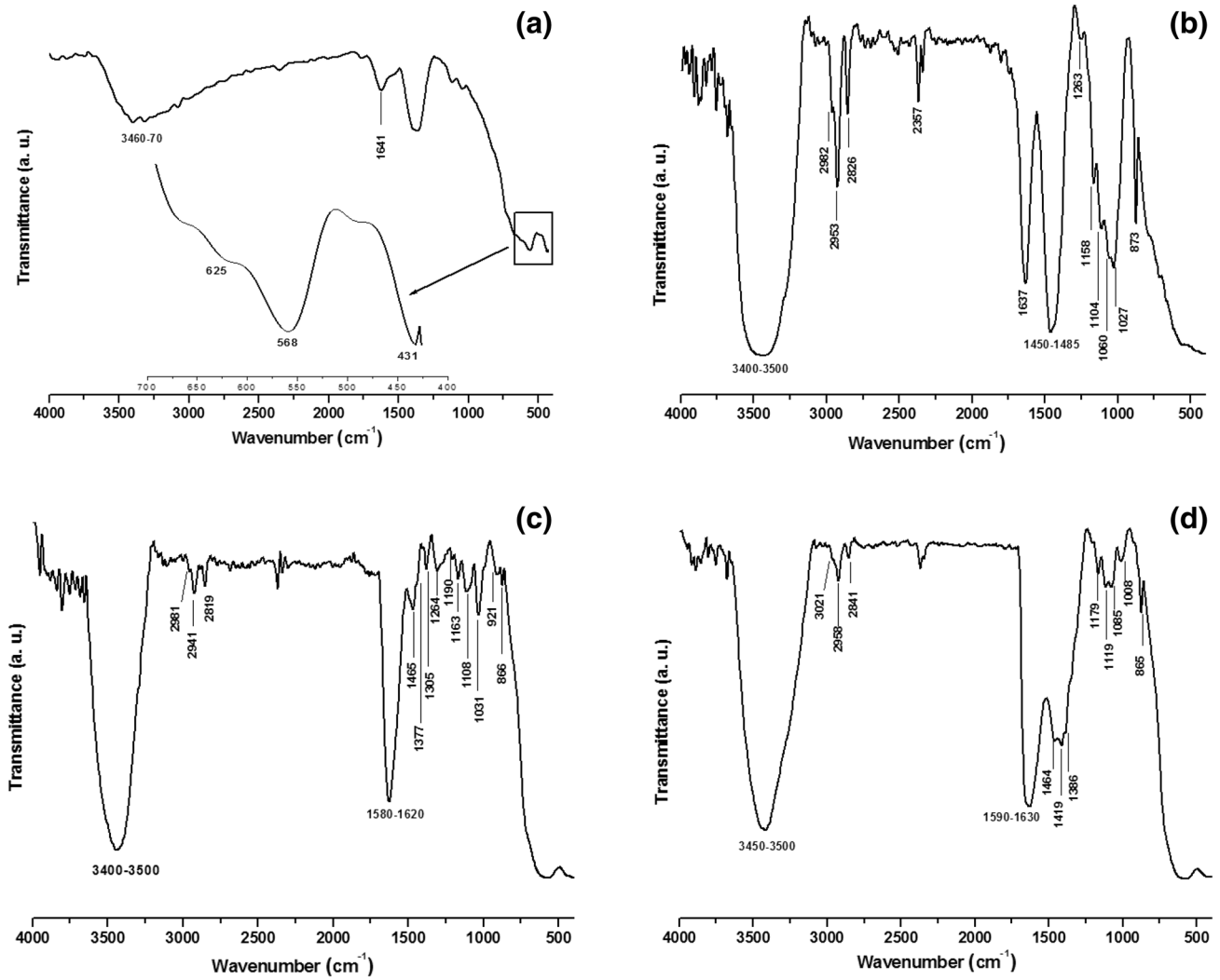

Fig. 4 IR spectra of the prepared **a** naked, **b** cysteine-, **c** glycine- and **d** glutamine-coated Fe_3O_4 nanoparticles

the phase and crystal structures of the electrodeposited particles in the presence of amino acids had not changed. Notably, there were some broadenings and a slight reduction in the intensity of the diffraction peaks of coated nanoparticles as compared with uncoated ones, which may be related to the smaller size of the coated Fe_3O_4 nanoparticles.

The average crystallite size (D) was calculated from the diffraction line-width of XRD patterns, based on the Scherrer's equation ($D = 0.9\lambda/\beta \cos(\theta)$), where, β is the full width at half maxima (FWHM) of the (311) peak. The calculations resulted average sizes of 9.1, 7.2, 7.6 and 8.1 nm for the uncoated, cysteine-, glycine- and glutamine-coated nanoparticles, respectively.

3.2 FE-SEM and TEM

Morphological characteristics of the electrosynthesized coated and uncoated Fe_3O_4 nanoparticles were observed through FE-SEM and TEM, sample results of which are presented in Figs. 2 and 3. The FE-SEM image (in Fig. 2a) of the uncoated Fe_3O_4 sample exhibits a particle-like morphology with some degree of agglomeration. The size of the agglomerated particles was estimated to be about 20 nm. High resolution observation through TEM (Fig. 3a) also indicated that the naked Fe_3O_4 particles were agglomerated and their size was about 10 nm. For the coated Fe_3O_4 samples, spherical particle morphology was observed as indicated in Fig. 2b–d. The mean diameter of the observed particles was 15 nm. It seems that the amino acid coated nanoparticles have smaller sizes as compared with the bare MNPs. TEM observations in Fig. 3b–d clearly revealed that the coated nanoparticles have better dispersion and lower agglomeration. This is due to the role of the coating agent during formation and growth of the Fe_3O_4 particle, where the coating layer, on the surface of the magnetite particles, prevents their agglomeration

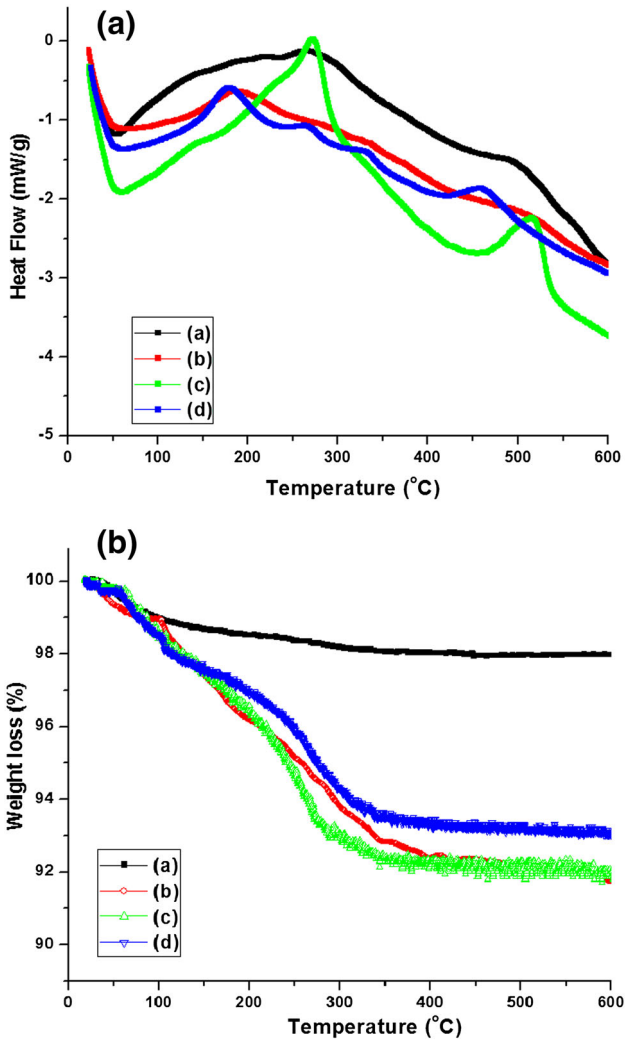

Fig. 5 **a** DSC and **b** related TG curves for the prepared **a** naked, **b** cysteine-, **c** glycine- and **d** glutamine-coated Fe_3O_4 nanoparticles

during their deposition time. The particle sizes were determined to be 8, 8, and 9 nm for the cysteine-, glycine- and glutamine-coated Fe_3O_4 particles, respectively. The observed particle sizes from the TEM results are very close to those calculated from the XRD patterns.

3.3 FT-IR

Figure 4 presents the IR spectra of the uncoated and coated MNPs. In the spectrum of the naked MNPs, the following vibration modes can be observed: the Fe–O vibrations in tetrahedral site located at 565 cm^{-1}, and Fe–O vibration at octahedral site at 431 cm^{-1} [10, 16–18]. Notably, the stretching vibration at 565 cm^{-1} has the shoulder around 615 cm^{-1} due to the slight oxidation of the NPs surface [10, 29, 46]. For amino acid coated MNPs, these vibrations are also observed at 585 and 439 cm^{-1}, respectively. It is worth noting that the shoulder peak is not seen in the coated MNPs, indicating the stable form of these prepared NPs. In the IR spectrum of naked NPs (Fig. 4a), two IR peaks are also observed at about 1640 and 3460 cm^{-1}, which are due to the deforming and stretching vibrations of OH groups and water molecules connected to the Fe_3O_4 surface. As the surface Fe atoms are unsaturated in aqueous medium they coordinate with OH^- ions or H_2O molecules.

For coated nanoparticles, there are several IR bands at the 1000–1650 and 2500–3400 cm^{-1}, which are related to the coated amino acids. For the cysteine-coated MNPs (Fig. 4b), the IR peaks included (1) a sharp band at 2357 cm^{-1} arising from the SH groups [22, 46], (2) 1325 and 2920–2850 cm^{-1} due to C–N and C–H stretching vibrations, (3) a broad band at 1628 cm^{-1} which can be ascribed to the N–H stretching vibrations, which indicates the presence of free amino group, (4), a peak at 2826 cm^{-1} corresponding to the N–H asymmetric stretching [14, 46, 47], (5) peaks at $\sim$1630 and $\sim$1439 cm^{-1} due to C=O and C–O stretching vibrations, (6) a sharp peak at 873 cm^{-1} indicating the C–S vibration [19, 21] and (7) the N–H stretching vibration overlaps with the stretching of OH at 3419 cm^{-1}. There coexisting IR absorption bands of $–COO^-$, $–NH_2$ were observed for L-cysteine-coated NPs. Therefore, it can be concluded that carboxylic acid and amino groups are present on the surface of the Fe_3O_4 nanoparticles.

For the glycine-coated MNPs, the IR spectrum in Fig. 4c reveals the following peaks; (1) a band at 2819 cm^{-1} corresponding to the asymmetric stretching of N–H [10, 19, 46], (2) two bands at 2941 and 2981 cm^{-1} related to CH_2 vibrations, (3) the relatively strong band at 1580–1620 cm^{-1} arising from the vibrations modes of C=O and NH_2 groups [14, 20, 46], (4) peaks at 1465 and 1377 cm^{-1} are due to the stretching vibrations of C–O and C–N, (5) the bands corresponding to the O–H vibration modes at 866 and 1031 cm^{-1}, (6) the bands at 1305, 1264 and 1163 cm^{-1} attributed to the vibrations of CH_2 group, (7), a broad peak at 3400–3500 cm^{-1} including the vibrations of the hydroxyl and amine groups, and (8) C–C vibration observed at 1108 cm^{-1}. These IR data confirmed the presence of glycine coating on the surface of MNPs.

The IR spectrum of the glutamine-coated MNPs (Fig. 4d) also exhibited the vibration bands relating to the NH_2, CH_2, C=O, COO, C–C, C–N, C–H and N–H, which confirms the successful coating of glutamine during the electrosynthesis.

3.4 TG–DTA

The presence of the amino acids (i.e., cysteine, glycine and glutamine) on the surface of the electrodeposited iron oxide nanoparticles can also be well demonstrated by the TG–DTA. This technique is also suitable for characterization

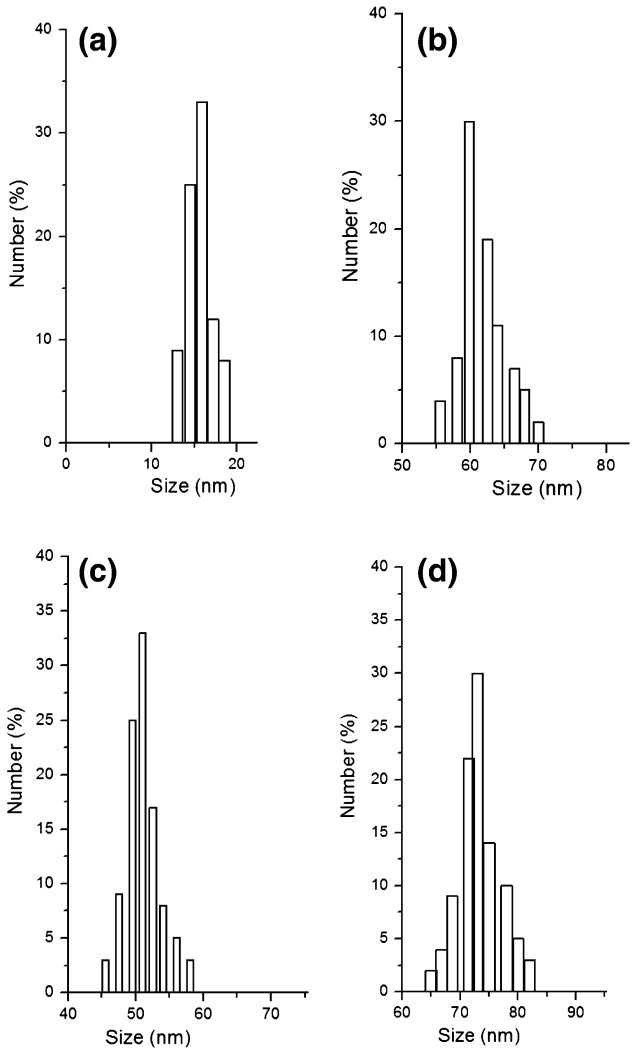

Fig. 6 DLS profiles of the prepared of the prepared **a** naked, **b** cysteine-, **c** glycine- and **d** glutamine-coated Fe_3O_4 nanoparticles

analyses for thermal characterization of nanoparticles and provides quantitative proof on the structure of the coating agents, and also allows us to determine the bonding strength of the coatings with the surface of iron oxide nanoparticles and their thermal stability. Generally, coating agents with strong chemical bonds are removed from the nanoparticles surface at higher temperatures. Figure 5 shows the typical TG–DTA diagrams of the prepared naked, as well as, cysteine-, glycine- and glutamine-coated iron oxide nanoparticles. From the TG–DTA diagrams it is observed that, there are three essential weight loss incidents. The first step happens at temperatures below 120 °C, where the DTA diagrams of both uncoated and coated nanoparticles exhibit a broad endothermic peak. This is due to the evaporation of residual water molecules present in the structure of the solid compounds and also the elimination of OH^- groups connected onto the surface of iron oxide nanoparticles. Accordingly, TG diagrams of all prepared nanoparticles have relative sharp weight losses in this temperature range. The weight loss values were about 1.95, 1.05, 1.43 and 1.5% for the naked, cysteine-, glycine- and glutamine-coated iron oxide nanoparticles, respectively. After 120 °C, the DTA and TG diagrams of the coated nanoparticles exhibited a different path as compared with those of the naked ones. This is related to the presence of amino acid coatings on the surface of iron oxide nanoparticles. For the naked nanoparticles, two peaks were observed on the DTA diagrams at 165 and 460 °C. These can be related to the oxidation and change in the crystal nature of Fe_3O_4 particles. In fact, Fe_3O_4 is converted into the γ-Fe_2O_3 and α-Fe_2O_3 phases at these temperatures [10, 11, 18, 29]. Notably, in the DCS diagrams of the coated Fe_3O_4 nanoparticles, the endothermic peaks at about 170–190 and 450–520 °C are related to the conversion of magnetite into maghemite and hematite phase. It has been reported that the location of these peak can be determined from the crystal size of the magnetite nanoparticles and type of the surface coating [46, 47].

The functionalized or coated Fe_3O_4 nanoparticles exhibited different thermogravimetric behaviors and weight loss values at the temperature range of 200–400 °C, as compared with the uncoated nanoparticles. The exothermic peaks on the DSC diagrams of coated nanoparticles were due to the decomposition of amino-acid coat layer on the surface of nanoparticles [10, 14, 19–21, 45, 47]. Notably, the location and intensity of these exothermic peaks is related to the type of amino acid, as it is clearly seen in Fig. 5a. Accordingly, the TG diagrams at this temperature range (i.e., 200–400 °C) show very sharp weight loss peaks. After this temperature range, no considerable weight loss phenomena were observed in the case of the three coated samples, indicating that the amino acid coating is eliminated from the sample surface over 400 °C. Total weight loss values of 8.32, 8.02 and 7.05 wt% are observed in the TG diagrams for the cysteine-, glycine- and glutamine-coated nanoparticles, while the total weight loss of the naked nanoparticles was about 2.01 wt% as seen in their TG diagram (Fig. 5b). Hence, the observed weight losses for coated particles can be mainly attributed to the coating agents on the surface of iron oxide nanoparticles [10–13, 16–22], confirming the efficient functionalization of Fe_3O_4 nanoparticles during electrosynthesis through cathodic electrodeposition.

3.5 Dynamic light scattering

Figure 6 shows the particle size distributions measured for the prepared iron oxide nanoparticles. For bare MNPs, the mean hydrodynamic diameter was measured to be $\sim$17 nm, which is rather larger than that determined based

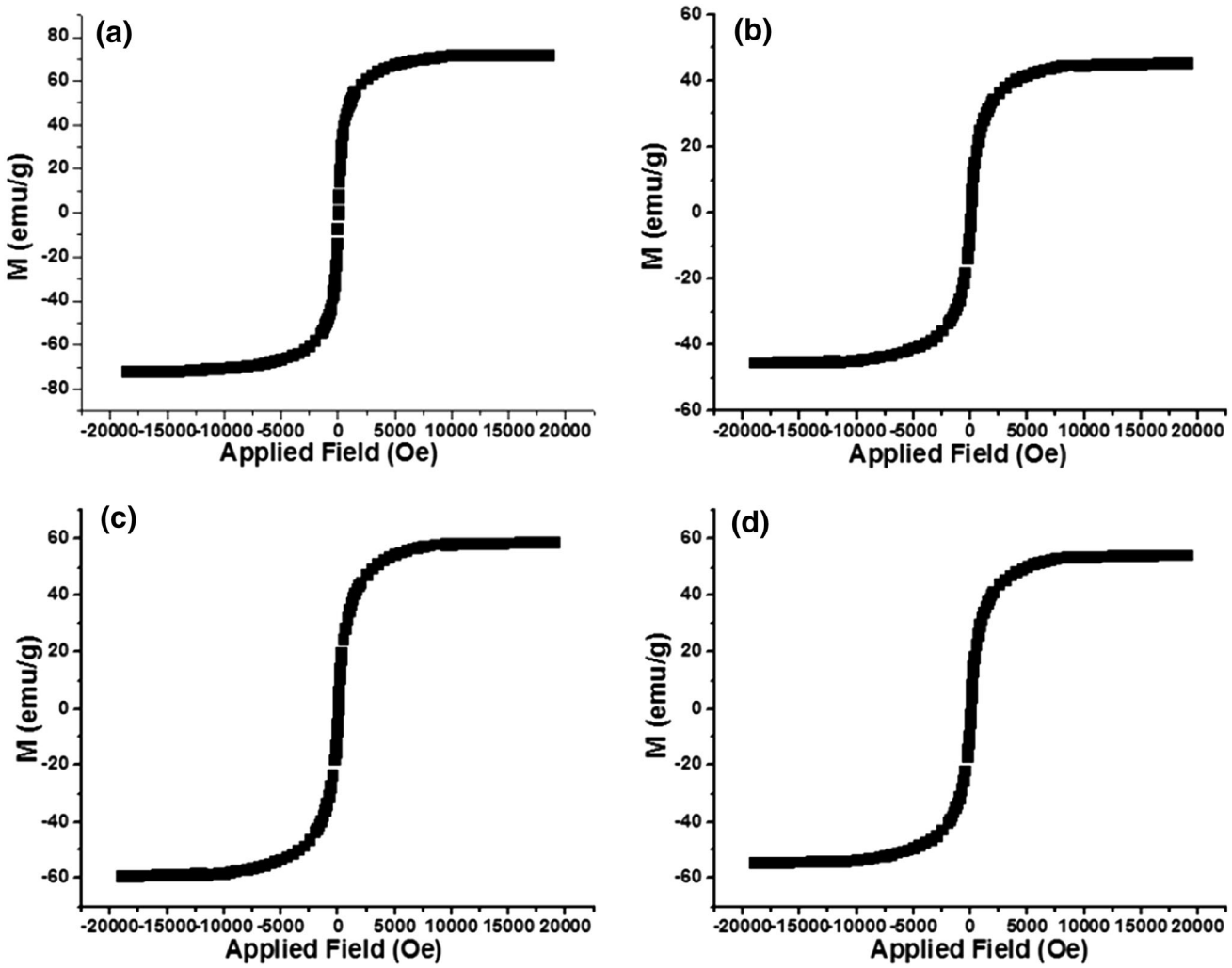

Fig. 7 Hysteresis profiles of the prepared of the prepared **a** naked, **b** cysteine-, **c** glycine- and **d** glutamine-coated Fe_3O_4 nanoparticles

Table 1 The magnetic properties of the prepared magnetite NPs

Sample name	Ms (emu g^{-1})	Mr (emu g^{-1})	Ce (Oe)
Naked MNPs	71.3	0.71	2.3
Cysteine coated MNPs	45.5	0.64	1.8
Glycine-coated MNPs	58.9	0.45	0.72
Glutamine-coated MNPs	54.6	0.55	1.1

on the TEM observations. This is due to the fact that DLS measurements are performed in the solution media, while TEM and FE-SEM are related to the particle size in dry state. The hydrodynamic diameters of the cysteine-, glycine and glutamine-coated MNPs were measured to be ~60, 50 and 72 nm, respectively. It can be seen that the coated particles have larger diameters than that of the uncoated ones. This increase in the hydrodynamic diameter clearly implies the presence of an amino acid coating layer on the surface of the electro-synthesized MNPs.

3.6 Magnetic evaluation

The magnetic evaluations of the prepared MNPs, were performed using vibrating sample magnetometery (VSM), within a magnetic field range of −20,000 to 20,000 Oe, and the magnetic properties studied included saturation magnetization (Ms), remnant magnetization (Mr) and coercivity (Ce) of all samples. Figure 7 presents the hysteresis curves of the prepared MNPs at room temperature. All VSM profiles exhibit completely reversible S shapes indicating the super-paramagnetic behavior of both coated and uncoated magnetite NPs. The Ms, Mr and Ce values of these samples are listed in Table 1.

From the magnetic data in Table 1, the following conclusions can be made:

- The saturation magnetization of iron oxide nanoparticles is reduced with coating, due to the diamagnetic nature of cysteine, glycine and glutamine.
- In contrast to the large reduction in Ms value by other biocompatible coatings such as polymers, organic acids and silica [2–9], the reductions observed for these coating agents have been low.
- The reduction in the magnetic saturation of the coated Fe_3O_4 nanoparticles is in agreement with the reports in the literature [11, 12, 19–22, 46, 47].
- The prepared MNPs exhibited negligible Mr and Ce values, which confirmed their superior super-paramagnetic nature.

4 Conclusion

Based on what has been discussed it can be concluded that bare and amino acid coated magnetite NPs could be successfully prepared through electrogeneration of hydroxide ions on the surface of a cathode. The morphological studies by FE-SEM and TEM showed that the prepared MNPs were spherical particles with an average diameter of 10 nm. XRD results confirmed that both uncoated and coated NPs had magnetite crystalline phase. The presence of the amino acid coating on the surface of the deposited MNPs was confirmed by TG, DLS and FT-IR analyses. The thermo-gravimetric analyses further exhibit 8.32, 8.02 and 7.05 wt% weight losses for the cysteine-, glycine- and glutamine- coated nanoparticles, upon thermal treatment. Investigations on the magnetic behavior of the coated MNPs confirmed that they had high saturation magnetization, and negligible remnant magnetization (Mr) and coercivity (Ce) values. In conclusion, the proposed cathodic deposition can be recognized as a facile technique for the in situ coating of amino acids on iron oxide nanoparticles.

Compliance with ethical standards

Conflict of interest The authors declare that there is no conflict of interest regarding the publication of this paper.

References

1. T. Yadavalli, D. Shukla, Nanomedicine **13**, 219 (2017)
2. I. Karimzadeh, H. Rezagolipour Dizaji, M. Aghazadeh, J. Magn. Magn. Mater. **416**, 81 (2016)
3. T. Zare, M. Lotfi, H. Heli, N. Azarpira, A.R. Mehdizadeh, N. Sattarahmady, M.R. Abdollah-dizavandi, M. Heidari, Appl. Phys. A **120**, 1189 (2015)
4. I. Karimzadeh, H. Rezagholipour Dizaji, M. Aghazadeh, Mater. Res. Express **3**, 095022 (2016)
5. I. Karimzadeh, M. Aghazadeh, M.R. Ganjali, T. Dourudi, Curr. Nanosci. **13**, 167 (2017)
6. I. Karimzadeh, M. Aghazadeh, M.R. Ganjali, P. Norouzi, S. Shirvani-Arani, T. Doroudi, P.H. Kolivand, S.A. Marashi, D. Gharailou, Mater. Lett. **179**, 5 (2016)
7. I. Karimzadeh, M. Aghazadeh, M.R. Ganjali, P. Norouzi, T. Doroudi, P.H. Kolivand, Mater. Lett. **189**, 290 (2017)
8. M. Aghazadeh, I. Karimzadeh, M.R. Ganjali, M. Mohebi, Morad. Mater. Lett. **196**, 392 (2017)
9. L. Casas, A.R.E. Molins, J.M. Grenèche, J. Asenjo, J. Tejada, Appl. Phys. A **74**, 591 (2002)
10. I. Karimzadeh, M. Aghazadeh, T. Doroudi, M.R. Ganjali, P.H. Kolivand, D. Gharaiolu, J. Cluster Sci. **28**, 1259 (2017)
11. Z.Z. Yu, Q.H. Wu, S.L. Zhang, J.Y. Miao, B.X. Zhao, L. Su, RSC Adv. **6**, 10159 (2016)
12. S. Theerdhala, D. Bahadur, S. Vitta, N. Perkas, Z. Zhong, A. Gedanken, Ultrason. Sonochem. **17**, 730 (2010)
13. D. Patel, Y. Chang, G.H. Lee, Curr. Appl. Phys. **9**, S32 (2009)
14. I. Karimzadeh, M. Aghazadeh, T. Doroudi, M.R. Ganjali, P.H. Kolivand, D. Gharailou, Curr. Nanosci. **3**, 274 (2017)
15. H. Hu, J. Sun, G. Huang, X. Li, A. Dai, H. Yang, J. Mater. Sci. **48**, 7686 (2013)
16. A. Ebrahiminezhad, V. Varma, S. Yang, Y. Ghasemi, A. Berenjian, Nanomaterials **6**, 1 (2016)
17. A. Ebrahiminezhad, S.R. Amini, S. Davaran, J. Barar, M. Moghadam, Y. Ghasemi, Curr. Nanosci. **10**, 382 (2014)
18. A. Ebrahiminezhad, S.R. Amini, S. Davaran, J. Barar, Y. Ghasemi, Bull. Korean Chem. Soc. **33**, 3957 (2012)
19. A. Ebrahiminezhad, S.R. Amini, S. Davaran, J. Barar, Y. Ghasemi, Curr. Nanosci. **11**, 113 (2015)
20. A. Ebrahiminezhad, Y. Ghasemi, S. Rasoul-Amini, J. Barar, S. Davaran, Colloids Surf. B **102**, 534 (2013)
21. Z. Wang, H. Zhu, X. Wang, F. Yang, X. Yang, Nanotechnology **20**, 465 (2009)
22. Z. Durmus, H. Kavas, M.S. Toprak, A. Baykal, T. Altincekic, A. Aslan, A. Bozkurt, S. Cosgun, J. Alloys Compd. **484**, 371 (2009)
23. R. Herrera-Becerra, C. Zorrilla, J.L. Rius, J.A. Ascencio, Appl. Phys. A **91**, 241 (2008)
24. R. Herrera-Becerra, J.L. Rius, C. Zorrilla, Appl. Phys. A **100**, 453 (2010)
25. J. Wan, G. Tang, Y. Qian, Appl. Phys. A **86**, 261 (2007)
26. D. Primc, B. Belec, D. Makovec, J. Nanopart. Res. **18**, 64 (2016)
27. M. Aghazadeh, M.R. Ganjali, P. Norouzi, J. Mater. Sci. Mater. Electron. **2**, 7707 (2016)
28. G.M. Bhalerao, A.K. Sinha, H. Srivastava, A.K. Srivastava, Appl. Phys. A **95**, 373 (2009)
29. E. Tuncer, A.J. Rondinone, J. Woodward, I. Sauers, D.R. James, A.R. Ellis, Appl. Phys. A **94**, 843 (2009)
30. M. JalalianS, M. Mirkazemi, S. Alamolhoda, Appl. Phys. A **122**, 835 (2016)
31. H.-J. Song, N. Li, X.-Q. Shen, Appl. Phys. A **102**, 559 (2011)
32. V. Panchal, U. Bhandarkar, M. Neergat, K.G. Suresh, Appl. Phys. A **114**, 537 (2014)
33. M. Aghazadeh, I. Karimzadeh, M.R. Ganjali, J. Mater. Sci. Mater. Electron. (2017). doi:10.1007/s10854-017-7192-z
34. X. Zeng, Z. Wang, y Liu, M. Ji, Appl. Phys. A **80**, 581 (2005)
35. M. Aghazadeh, M. Asadi, M.R. Ganjali, P. Norouzi, B. Sabour, M. Emamalizadeh, Thin Solid Films **634**, 24 (2017)
36. M. Aghazadeh, M.R. Ganjali, P. Norouzi, Mater. Res. Express **3**, 055013 (2016)
37. M. Aghazadeh, M. Hosseinifard, Ceram. Int. **39**, 4427 (2013)
38. M. Aghazadeh, A.A. Malek Barmi, H.M. Shiri, S. Sedaghat, Ceram. Int. **39**, 1045 (2013)
39. M. Aghazadeh, B. Arhami, A.A. Malek Barmi, M. Hosseinifard, D. Gharailou, Mater. Lett. **115**, 68 (2014)
40. M. Aghazadeh, M. Hosseinifard, B. Sabour, S. Dalvand, Appl. Surf. Sci. **287**, 187 (2013)

41. J. Talat Mehrabad, M. Aghazadeh, M. Ghannadi Maragheh, M.R. Ganjali, P. Norouzi, Mater. Lett. **184**, 223 (2016)
42. M. Aghazadeh, B. Sabour, M.R. Ganjali, S. Dalvand, Appl. Surf. Sci. **313**, 581 (2014)
43. M. Aghazadeh, S. Dalvand, M. Hosseinifard, Ceram. Int. **40**, 3485 (2014)
44. F. Khosrow-pour, M. Aghazadeh, B. Sabour, S. Dalvand, Ceram. Int. **39**, 9491 (2013)
45. F. Abed, M. Aghazadeh, B. Arhami, Mater. Lett. **99**, 11 (2013)
46. A.B. Salunkhe, V.M. Khot, J.M. Rusoc, S.I. Patil, RSC Adv. **5**, 18420 (2015)
47. D. Rehana, A.K. Haleel, A.K. Rahimana, J. Chem. Sci. **127**, 1155 (2015)